



Microfluidic capture of selected biomolecules with functionalized particles. Design under a numerical approach

Gloria González-Lavín , Christian Fernández-Maza , Lucía Gómez-Coma ,
Marcos Fallanza , Inmaculada Ortiz 

Departamento de Ingenierías Química y Biomolecular, Universidad de Cantabria, Av. Los Castros s/n, 39005 Santander, Spain

ARTICLE INFO

Keywords:

CFD
Engineered proteins
Eulerian/Lagrangian model
LPS capture
Microfluidics
Solid/liquid

ABSTRACT

The outstanding capabilities of S/L functionalized particulate systems synergized with microfluidics offer great opportunities to address current and significant challenges, as the selective capture of biomolecules from a liquid phase, a process highly reliant on the intimate contact between both phases. In this work, we report the numerical prediction of the selective sequestration of a target biomolecule present in an aqueous solution onto engineered solid capture agents. For this purpose, a customized Eulerian/Eulerian/Lagrangian model able to track all the phases involved in the system and account for the S/L interfacial mass transfer has been developed. The challenging capture of endotoxins (LPS), sepsis causing agents, by solid beads decorated with engineered binding proteins has been selected as motivating case study. The computational tool has been successfully validated using batch data previously reported by our research group with capture deviations inferior to 5 %. Furthermore, we advance the design of microdevices to continuously withdraw LPS from biofluids and promote those variables with influence on the rate of the interfacial mass transfer. The design procedure has rendered a coil inspired T-type microreactor that displays an exceptional performance. This device can treat 1.4 L per hour of a sample containing $1 \text{ mg}\cdot\text{mL}^{-1}$ LPS, attain the fluids complete mixing in less than 5 s, a uniform particle distribution and reach the LPS capture equilibrium in less than 15 s. Thus, to the best of our knowledge, we report herein for the first time the design of advanced microdevices for toxin removal assisted by a Euler/Euler/Lagrange model.

1. Introduction

Heterogeneous systems comprising a particulate solid phase are in vogue. Their performance and versatility are reinforcing and pushing forward their implementation in already proven applications and propelling them into the exploration of new uses, making these systems a great value in a vast array of scenarios. Among all the areas in which solid/liquid particulate systems are finding a niche, biomedical applications are currently garnering increased attention through biosensing [1,2], drug delivery [3,4] or pathogens removal [5,6]. These applications are commonly framed in a synergy with microfluidics, given the remarkable features that this field offers. Enhancements in mass and heat transport, reduced and precisely controlled residence times, lower sample or reagents consumption and more accurate control over the trajectories of the particles represent the primary benefits that microfluidics offers [7–10].

The development of accurate and robust numerical models that

predict precisely the behavior of real systems is an excellent asset to tackle the design, evaluation and testing of S/L systems prior to the experimental implementation, which requires an investment in resources as manufacturing materials, reagents and time [11]. When designing systems bound to enclose solid/liquid microfluidic reactive separations, having a model that provides a faithful depiction of the position in time and space of each component can become of primary importance. To generate reliable outcomes and be a solid basis on which a new design can be built, the mathematical tool must not only reproduce the direct contact between phases, but also the interfacial mass transfer rate that rules the separation process. Several options arise to model S/L particulate flows [12] and the phenomena derived from that contact, being the Euler/Lagrange approach the one that guarantees the continuous location of all the components implied in the system [13].

The Euler/Lagrange framework describes the fluid phase as a continuum medium whose motion is ruled by the conservation equations. Meanwhile, the particulate phase is portrayed under the Lagrangian reference frame as a discrete ensemble formed by a set of individual

* Corresponding author.

E-mail address: ortizi@unican.es (I. Ortiz).

<https://doi.org/10.1016/j.cej.2025.100747>

Nomenclature	
<i>Roman symbols</i>	
A	Surface (m^2)
c	Molar concentration ($kmol \cdot m^{-3}$)
C_D	Drag coefficient (–)
C_{vm}	Virtual mass factor (–)
d	Diameter (m)
d_{ij}	Deformation rate tensor (s^{-1})
D_{i, m}	Mass diffusion coefficient of species <i>i</i> in the medium <i>m</i> ($m^2 \cdot s^{-1}$)
D_{T, i}	Thermal diffusion coefficient for species <i>i</i> ($kg \cdot m^{-1} \cdot s^{-1}$)
F	Force ($kg \cdot m \cdot s^{-2}$)
g	Gravity vector ($m \cdot s^{-2}$)
I	Unit tensor (–)
J_i	Diffusion flux of species <i>i</i> ($kg \cdot m^{-2} \cdot s^{-1}$)
k	Equilibrium ratio ($m^3 \cdot kg^{-1}$)
k_f	Mass transfer coefficient ($m \cdot s^{-1}$)
K_{eq}	Equilibrium constant ($m^3 \cdot mol^{-1}$)
K_S	Coefficient of Saffman's lift force (–)
LPS	Lipopolysaccharide
LPS – P	LPS-LALF protein complex
m	Mass (kg)
m_{k,i}	Mass flow rate of species <i>i</i> in cell <i>k</i> ($kg \cdot s^{-1}$)
MI	Mixing Index (–)
N	Number of sampling points
p	Pressure ($kg \cdot m^{-1} \cdot s^{-2}$)
P	LALF protein
Pe	Peclet number (–)
Q_{i, 1}	Mass fraction of species <i>i</i> on the solid (–)
Re	Reynolds number (–)
S_i	Species source term ($kg \cdot m^{-3} \cdot s^{-1}$)
S_m	Mass source term ($kg \cdot m^{-3} \cdot s^{-1}$)
S_{mom}	Momentum source term ($kg \cdot m^{-3} \cdot s^{-1}$)
Sh	Sherwood number (–)
S/L	Solid/liquid
t	Time (s)
T	Temperature (K)
v	Velocity vector ($m \cdot s^{-1}$)
V	Volume (m^3)
x	Position vector (m)
Y_i	Mass fraction of species <i>i</i> (–)
<i>Greek symbols</i>	
α	Volume fraction (–)
γ	Mass concentration ($kg \cdot m^{-3}$)
μ	Dynamic viscosity ($kg \cdot m^{-1} \cdot s^{-1}$)
ν	Kinematic viscosity ($m^2 \cdot s^{-1}$)
ρ	Density ($kg \cdot m^{-3}$)
τ	Stress tensor ($kg \cdot m^{-1} \cdot s^{-2}$)
τ	Residence time (s)
τ_r	Particle relaxation time (s)
φ	Mass ratio protein per LPS ($kg_P \cdot kg_{LPS}^{-1}$)
ω	Angular velocity ($rad \cdot s^{-1}$)
<i>Subscripts</i>	
eq	Relative to the equilibrium
i	<i>i</i> -th species
k	<i>k</i> -th cell
m	<i>m</i> -th medium
part	Relative to particle
q	<i>q</i> -th phase

particles whose path along the computational domain is found by solving the Newtonian equations of motion [12,14]. This approach is proven as a very useful tool to investigate the hydrodynamic behavior of particulate flows and allows for the handling of complex phenomena as particle size or composition [15]. Models based on this approach have been reported to study the dispersion and deposition of aerosols [16,17], erosion [18], separation of phases [19,20], combustion [21], adsorption [22] or UV deactivation of bacteria [23]. Evidence of the use of Eulerian/Lagrangian models to depict the operation of microfluidic biosystems can be found in the literature. However, current research works are mainly focused on describing the path of the discrete phase (such as cells) or their physical separation [24–26]. Meanwhile, the development of S/L models that incorporate phenomena beyond flow and physical forces for the sequestration of molecules has not yet been fully explored.

Hence, it becomes necessary to fill this gap and make available rigorous models able to predict all the phenomena implied in the S/L interaction in microfluidic reactive biosystems. Thus, the development of efficient and selective analytical microprocesses, the design of microdevices to carry out these processes with outstanding performance and the selection of operational variables that improve the outcomes would be supported and countersigned by a solid and powerful tool.

With the purpose of advancing on the availability of versatile models that depict the fast analysis, detection and capture of pathogens in biofluids, this work presents a Euler/Lagrange based model that accounts for the selective binding and microfluidic sequestration of endotoxins onto engineered proteins supported on beads. For that purpose, a previous work from the research group [27,28] is taken as starting point. Basauri et al. developed an integrated methodology merging protein and chemical engineering fundamentals to propose an effective and economically viable molecule to sequester LPS, a potential trigger

in the pathogenesis of sepsis. With that end, the authors engineered an anti-lipopolysaccharide factor (LALF) protein, anchored this newly synthesized molecule onto agarose beads and performed batch LPS capture experiments. Starting from this data, the work herein presented develops a Eulerian/Eulerian/Lagrangian model to prove its proficiency in the prediction of the performance of S/L reactive systems and builds up to show the versatility of the computational tool by assisting the design of microdevices to be applied in the microfluidic fast and continuous capture of target molecules.

2. Development of the mathematical model

2.1. Continuous phase modeling

In this work, the Eulerian/Lagrangian approach is applied to predict the LPS capture by functionalized beads in two scenarios; (i) in batch mode inside a sealed Eppendorf® tube that contains two continuous phases (air and the LPS solution) and the discrete one (functionalized beads) (Fig. 1a.), and (ii) in continuous mode inside a conveniently designed microdevice which contains only a single continuous liquid phase (the LPS solution) and the particulate one (Fig. 1b.). To track the interface between the two continuous phases in the Eulerian framework, the Volume of Fluid (VOF) model is employed. This Euler/Euler model allows to locate the interphase in those computational cells in which the volume fraction α_q (–) of one fluid phase *q* in a cell presents a value between 0 and 1. Scenario (i) demands the definition of this parameter to allocate the gas and liquid phases in the computational domain, resulting in a Eulerian/Eulerian/Lagrangian model. Meanwhile, scenario (ii) presents a single continuous phase and α presents a value of 1 for the liquid phase in the whole domain, leading to a Eulerian/

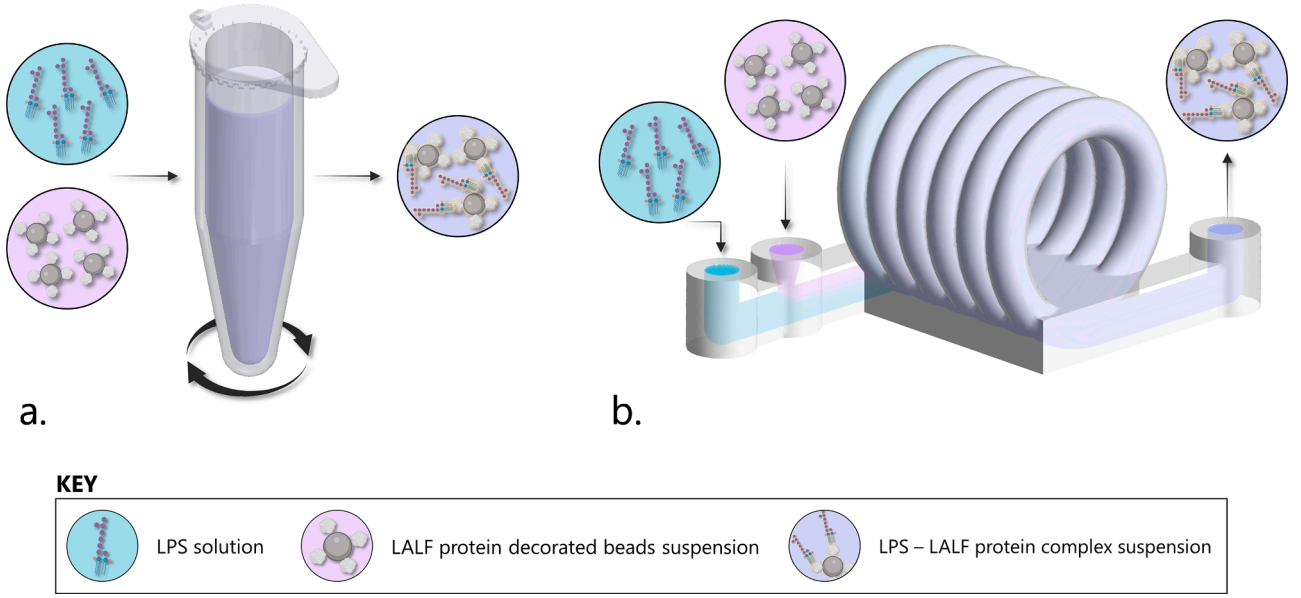


Fig. 1. Conceptualization of the modeled LPS sequestration scenarios: a. Batch capture in a stirred Eppendorf® tube and b. Continuous removal in a microdevice.

Lagrangian based model.

The proposed model solves the laminar and incompressible continuous flow using the Navier-Stokes equations, which govern mass and momentum conservation:

$$\frac{\partial}{\partial t}(\alpha_q \rho_q) + \nabla \cdot (\alpha_q \rho_q \vec{v}_q) = S_{m,q} \quad (1)$$

$$\frac{\partial}{\partial t}(\alpha_q \rho_q \vec{v}_q) + \nabla \cdot (\alpha_q \rho_q \vec{v}_q \vec{v}_q) = -\alpha_q \nabla \cdot \vec{p} + \nabla \cdot \vec{\tau}_q + \alpha_q \rho_q \vec{g} + S_{mom,q} \quad (2)$$

where ρ ($\text{kg}\cdot\text{m}^{-3}$) is the density, \vec{v} ($\text{m}\cdot\text{s}^{-1}$) is the velocity vector, p ($\text{kg}\cdot\text{m}^{-1}\cdot\text{s}^{-2}$) is the static pressure and \vec{g} ($\text{m}\cdot\text{s}^{-2}$) is the gravity force. S_m ($\text{kg}\cdot\text{m}^{-3}\cdot\text{s}^{-1}$) and S_{mom} ($\text{kg}\cdot\text{m}^{-2}\cdot\text{s}^{-2}$) represent the mass and momentum source terms resulting from the interfacial contact between fluid and solid phases, respectively. Meanwhile, $\vec{\tau}$ is the stress tensor ($\text{kg}\cdot\text{m}^{-1}\cdot\text{s}^{-2}$), given by:

$$\vec{\tau} = \mu_q \left[\alpha_q (\nabla \cdot \vec{v}_q + \nabla \cdot \vec{v}_q^T) - \frac{2}{3} \alpha_q \nabla \cdot \vec{v}_q I \right] \quad (3)$$

where μ ($\text{kg}\cdot\text{m}^{-1}\cdot\text{s}^{-1}$) is the dynamic viscosity and I (-), the unit tensor.

An additional conservation equation is considered to address the mixing and transport of chemical species within the system. This equation accounts for the effects of convection, diffusion and interfacial mass transfer.

$$\frac{\partial}{\partial t}(\alpha_q \rho_q Y_{i,q}) + \nabla \cdot (\alpha_q \rho_q \vec{v}_q Y_{i,q}) + \nabla \cdot \alpha_q \vec{J}_{i,q} = \alpha_q S_{i,q} \quad (4)$$

Being \vec{J}_i ($\text{kg}\cdot\text{m}^{-2}\cdot\text{s}^{-1}$) the diffusion flux of species i , $Y_{i,q}$ (-) the mass fraction of species i on phase q and S_i ($\text{kg}\cdot\text{m}^{-3}\cdot\text{s}^{-1}$) the source term corresponding to species i due to mass transfer between continuous and discrete phases. The diffusion flux, described through the Fick's law, is expressed as:

$$\vec{J}_{i,q} = -\rho_q D_{i,m} \nabla \cdot Y_{i,q} - D_{T,i} \frac{\nabla \cdot T}{T} \quad (5)$$

where $D_{i,m}$ ($\text{m}^2\cdot\text{s}^{-1}$) denotes the mass diffusion coefficient for species i in the fluid, T (K) is the temperature and $D_{T,i}$ ($\text{kg}\cdot\text{m}^{-1}\cdot\text{s}^{-1}$) is the Soret diffusion coefficient. The energy contributions are disregarded, as the system is assumed to be run under isothermal conditions.

The coupling between the continuous and discrete phases, involving mass, species and momentum, is facilitated by defining the so-called source terms. These variables aggregate all the volume-averaged contributions of all particles within each control volume.

$$S_m = -\sum_k \frac{\dot{m}_k}{V_{cell,k}} \quad (6)$$

$$S_i = -\sum_k \frac{\dot{m}_{k,i}}{V_{cell,k}} \quad (7)$$

$$S_{mom} = -\sum_k \frac{\vec{v}_k \dot{m}_k}{V_{cell,k}} - \sum_{i,k} \frac{\vec{F}_{i,k}}{V_{cell,k}} \quad (8)$$

Where \dot{m}_k ($\text{kg}\cdot\text{s}^{-1}$) the mass flow rate in cell k , $\dot{m}_{k,i}$ ($\text{kg}\cdot\text{s}^{-1}$) the mass flow rate of species i in cell k , $\vec{F}_{i,k}$ ($\text{kg}\cdot\text{m}^{-1}\cdot\text{s}^{-2}$) force i in cell k and $V_{cell,k}$ (m^3) is the volume of cell k .

2.2. Discrete phase modeling

The model herein reported is intended for applications with particle dilute flow, which implies managing particle volume fractions inferior to 12 % [29]. Hence, to approach the behavior of the particulate receptor phase the Discrete Phase Model (DPM) is selected. This model is based on the Lagrangian approach, which locates the particles in time and space by considering all the forces applied on them. Therefore, the path followed by each particle is predicted by solving the coupled trajectory and motion equations:

$$\frac{d\vec{x}_{part}}{dt} = \vec{v}_{part} \quad (9)$$

$$m_p \frac{d\vec{v}_{part}}{dt} = \vec{F}_{drag} + \vec{F}_{buoyancy} + \vec{F}_{virtual\ mass} + \vec{F}_{pressure\ grad.} + \vec{F}_{S.\ lift} \quad (10)$$

where \vec{x}_{part} (m) is the position of the particle, \vec{v}_{part} ($\text{m}\cdot\text{s}^{-1}$) denotes the velocity of the particle and m_{part} (kg) corresponds to the mass of the particle. Eq. (10) provides the force balance for each particle. The left part of the equation accounts for the particle inertia, while the right side for the external forces, which are given by:

$$\vec{F}_{drag} = m_{part} \frac{\vec{v} - \vec{v}_{part}}{\tau_r} \quad (11)$$

$$\vec{F}_{buoyancy} = m_{part} \frac{\vec{g}(\rho_{part} - \rho)}{\rho_{part}} \quad (12)$$

$$\vec{F}_{virtual\ mass} = C_{vm} m_{part} \frac{\rho}{\rho_{part}} \left(\vec{v}_{part} \nabla \vec{v} - \frac{d\vec{v}_{part}}{dt} \right) \quad (13)$$

$$\vec{F}_{pressure\ grad.} = m_{part} \frac{\rho}{\rho_{part}} (\vec{v} \nabla \vec{v}) \quad (14)$$

$$\vec{F}_{s.\ lift} = m_{part} \frac{2K_S \nu^{0.5} \rho d_{ij}}{\rho_{part} d_{part} (d_{ik} d_{kl})^{0.25}} (\vec{v} - \vec{v}_{part}) \quad (15)$$

τ_r (s) denotes the particle relaxation time, calculated using Eq. (16), ρ_{part} ($\text{kg}\cdot\text{m}^{-3}$) is the density of the particles, C_{vm} (–) is the virtual mass factor (which receives a value of 0.5), K_S (–) is the constant coefficient of Saffman's lift force (with a value of 2.594), ν ($\text{m}^2\cdot\text{s}^{-1}$) is the kinematic viscosity and d_{ij} (s^{-1}) is a deformation rate tensor [30]. In the selected simulation case, as the density ratio between the fluid (liquid) and the particles is greater than 0.1, the virtual mass and the pressure gradient forces are considered. The Saffman lift force given by Eq. (15) is considered as the particles present small Reynolds numbers [19].

$$\tau_r = \frac{\rho_{part} d_{part}}{18\mu} \frac{24}{C_D Re} \quad (16)$$

where, C_D (–) is the drag coefficient and Re denotes the relative Reynolds number. They can be found resorting to Eqs. (17) and (18), respectively. The beads are considered spherical, rigid and non-rotating.

$$C_D = a_1 + \frac{a_2}{Re} + \frac{a_3}{Re^2} \quad (17)$$

$$Re \equiv \frac{\rho d_{part} |\vec{v}_{part} - \vec{v}|}{\mu} \quad (18)$$

Here a_1 (–), a_2 (–) and a_3 (–) are constants dependent on the Reynolds number [31].

The mass transfer rates between the liquid solution initially containing the target biomolecule and the discrete beads decorated with capturing agents can be figured out employing Eq. (19), considering that a single species i is selectively exchanged. These interphase mass transfer rates are considered in the mass and species source terms provided by Eqs. (6) and (7).

$$\frac{dm_{part}}{dt} = \frac{dm_{part,i}}{dt} = A_{part} k_f \rho (Y_i - Y_{i,1}) \quad (19)$$

Here, A_{part} (m^2) corresponds to the superficial area of the beads, k_f ($\text{m}\cdot\text{s}^{-1}$) denotes the mass transfer coefficient, while Y_i (–) and $Y_{i,1}$ (–) represent the mass fraction of species i on the bulk of the fluid and at equilibrium with the solid, respectively.

To define the chemical equilibrium, a partition coefficient, shown in Eq. (20), is employed.

$$Q_{i,1} = Y_{i,1} k \quad (20)$$

Where $Q_{i,1}$ (–) is the mass fraction of species i on the surface of the beads and k ($\text{m}^3\cdot\text{kg}^{-1}$), the equilibrium ratio.

The calculation of the mass transfer coefficient is entrusted to a

correlation reported specifically for small particle Reynold's numbers [32]:

$$Sh = \frac{k_f d_{part}}{D_{i,m}} = 0.992 b^{1/3} Pe^{1/3} \quad (21)$$

Where, b (–) is a parameter dependant on the void fraction and Sh (–) and Pe (–) represent the Sherwood and Peclet dimensionless numbers, respectively.

The model herein reported has been implemented in the software ANSYS FLUENT 2019 R3 (ANSYS, Inc., Canonsburg, PA, USA). Eqs. (19), (20) and (21) have been incorporated separately in the software via a submodule coded in C language. This subroutine is crucial to track the beads along the computational domain and account for the mass transfer when the particles and the solution containing LPS are contacted. For this purpose, it is also imperative to solve the model under a two-way coupling approach [13]. Hence, the interactions between the solid and liquid, in both directions, are considered.

The flow field is solved resorting to the pressure-based segregated algorithm SIMPLE. The convective and diffusion terms are discretized using the second-order upwind scheme. Meanwhile, the gradient terms are assessed through the least squares cell-based scheme. The simulations herein presented have been performed in the Altamira Supercomputer at the Institute of Physics of Cantabria (IFCA-CSIC) and in a workstation with two processors Intel® Xeon® Gold 6148 and 256 GB RAM.

2.3. Studied scenarios

The main target of the model is to depict the selective sequestration of LPS from an aqueous solution onto functionalized particles. Following the mechanism proposed by [33], its removal is governed by (R1).



Where P refers to the binding protein (functional group anchored to the solid particles), LALF protein in this work, that can be found bonded to the beads and $LPS - P$ represents the resulting LPS-LALF protein complex, also linked to the particles. The preceding research work [27] proposed the equilibrium constant presented in Eq. (22), which serves as starting point to obtain the value of the equilibrium ratio k .

$$K_{eq} = \frac{[LPS - P]}{[LPS][P]} \quad (22)$$

Being $[LPS]$ (M), $[P]$ (M) and $[LPS - P]$ (M) the molar concentrations of LPS, LALF protein and LPS-LALF protein complex, respectively and K_{eq} (M^{-1}) the equilibrium constant.

The selective removal of LPS has been mathematically reproduced under batch and continuous operation mode. Both scenarios have been simulated under room temperature (20 °C) and the density and viscosity of the liquid phase were set as $998.2 \text{ kg}\cdot\text{m}^{-3}$ and $10^{-3} \text{ kg}\cdot\text{m}^{-1}\cdot\text{s}^{-1}$, respectively. In the case of scenario (i), the gaseous phase was assigned a density of $1.225 \text{ kg}\cdot\text{m}^{-3}$ and a viscosity of $1.785\cdot 10^{-5} \text{ kg}\cdot\text{m}^{-1}\cdot\text{s}^{-1}$. To the diffusivity of LPS in water was given a value of $3\cdot 10^{-11} \text{ m}^2\cdot\text{s}^{-1}$ and the equilibrium ratio that governs the LPS capture is, based on the research data published in [27], $1.1 \text{ m}^3\cdot\text{kg}^{-1}$. The micrometric particles injected in the system present a density of $1200 \text{ kg}\cdot\text{m}^{-3}$ and a protein charge of $42 \text{ g}_{protein}\cdot\text{g}_{part}^{-1}$.

To replicate the experimental results reported by Basauri et al. [27], the LPS capture is simulated in an Eppendorf® tube (Fig. 2a.). More detail about the engineered capture agents can be found in the Supplementary Material. To solve the system under batch mode, the

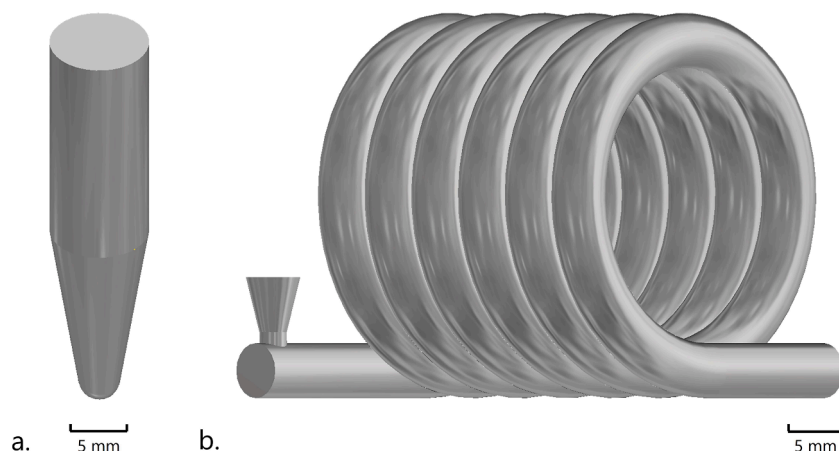


Fig. 2. a. Eppendorf® tube geometry employed in scenario (i) (batch removal). b. Coil inspired microdevice with T-shaped inlet employed in scenario (ii) (continuous removal).

computational domain is initialized so the simulated system perfectly matches the experimental conditions presented in the research in which this work is based on. This implies loading the tube with 1 mL of a solution presenting an LPS concentration of $0.5 \text{ mg}\cdot\text{mL}^{-1}$ and a certain charge of $45 \text{ }\mu\text{m}$ beads that matches a range of protein:LPS ratios, as defined by Eq. (23). Table 1 shows the selected ratios. The remaining tube volume is filled with air up to a total volume of 1.7 mL.

$$\phi = \frac{\gamma_P V_P}{\gamma_{LPS} V_{LPS}} \quad (23)$$

ϕ (–) denotes the protein:LPS ratio, γ_{LPS} ($\text{g}\cdot\text{L}^{-1}$) and γ_P ($\text{g}\cdot\text{L}^{-1}$) correspond to the mass concentration of LPS and protein and V_{LPS} (L) and V_P (L) define the volume of LPS solution and protein suspension.

Since the phases inside the Eppendorf® tube were experimentally stirred resorting to a vortex mixer, to reproduce the vigorous mixing the following description of the tube's movement is included in the model [34]:

$$v_x(t) = -\frac{d}{2}\omega \sin(\omega t) \quad (24)$$

$$v_z(t) = \frac{d}{2}\omega \cos(\omega t) \quad (25)$$

Where $v_x(t)$ ($\text{m}\cdot\text{s}^{-1}$) and $v_z(t)$ ($\text{m}\cdot\text{s}^{-1}$) are the velocities in the x and z components at time t (s), d (m) is the circling diameter and, ω ($\text{rad}\cdot\text{s}^{-1}$) is the angular velocity. The circling diameter is a parameter dependant on the vortex mixer model that indicates the diameter of the circular motion that the equipment creates when mixing. In this case, the tube is stirred in a vortex mixer with a circling diameter of 4.5 mm and an angular velocity of 1500 rpm. This geometry has been meshed using the MultiZone method resulting in a grid with by $2\cdot 10^4$ nodes, $4\cdot 10^3$ elements and presents a mesh skewness of 0.287 ± 0.241 .

To explore the versatility of the model in the design of microdevices, the mixing promotion using a coil inspired device with a T-shaped inlet is analyzed in scenario (ii) for the continuous removal of the toxin. The resulting reactor presents a total length of 600 mm

Table 1

Concentration of LPS capturing agents employed in the batch capture experiments.

ϕ	Concentration of particles ($\text{g}\cdot\text{L}^{-1}$)	Number of particles
35.6	0.42	$7.40\cdot 10^3$
53.4	0.64	$1.11\cdot 10^4$
89.0	1.06	$1.85\cdot 10^4$
392.4	4.67	$8.15\cdot 10^4$
456.4	5.43	$9.49\cdot 10^4$

and a diameter of 5 mm. The coil based microreactor is presented in Fig. 2b. This microdevice is meshed including a sphere of influence in the junction of both streams. It has been checked that a mesh including 10^5 nodes, $5\cdot 10^5$ elements and a skewness value of 0.218 ± 0.115 offers an adequate tradeoff between accuracy and computational solving time.

In this second scenario a liquid solution containing $1 \text{ mg}\cdot\text{mL}^{-1}$ of LPS is pumped at $0.02 \text{ m}\cdot\text{s}^{-1}$ through one inlet, while through the other inlet a suspension of $10 \text{ }\mu\text{m}$ particles with a charge of proteins corresponding to a ϕ of 456.4 is introduced at $0.02 \text{ m}\cdot\text{s}^{-1}$. In this situation, the system encloses a total of $1.12\cdot 10^6$ beads. The prediction of capture accuracy of the Euler/Lagrange model has already been tested using another chemical system in a preceding work [13].

3. Batch capture of target species. Model validation

Firstly, the accuracy and reliability of the presented model are proven by reproducing scenario (i): the batch experimental outcomes reported by Basauri et al. [27]. Fig. 3 shows the LPS mass fraction contours in the liquid phase rendered by the tool and found in the interior of the microtube at different ϕ values.

The contours displayed in Fig. 3 reveal how a greater ϕ influences positively the LPS removal extent, which is confirmed both theoretically and experimentally. The LPS capture in the microtubes is simulated under vigorously stirring conditions, which leads to the displacement of the air in the whole domain, being its position found in Fig. 3 in those

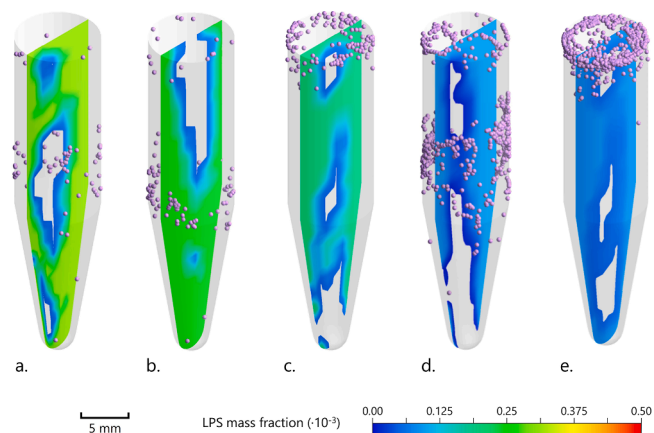


Fig. 3. LPS mass fraction contours under equilibrium conditions. a. $\phi = 35.6$, b. $\phi = 53.4$, c. $\phi = 89$, d. $\phi = 392.4$ and e. $\phi = 456.4$.

zones with grey colour. This representation is the result of displaying the LPS concentration field in a range between an infinitesimal value and the initial LPS concentration so the position of both phases (air and liquid) can be appreciated at the same time. The purple spheres correspond to the particles. Fig. 4 depicts quantitatively the predicted

toxin removal for the different operational conditions under analysis. With these results it is proven that the model is able to reproduce with an excellent accuracy the capture performance of the system. The precision of the mathematical tool is endorsed by a deviation between experimental and simulated data inferior to 5 %.

4. Continuous capture of target species. Advanced design of S/L microfluidic separation

To upgrade the batch mechanically stirred sequestration to a continuous approach based in passive agitation, it is crucial the selection of the most adequate geometry of the microcontactor. An efficient and fast separation depends on a geometry able to (i) promote fluid mixing and, (ii) facilitate the homogenous distribution of the beads in the channel. Hence, the rate of the contact between LPS molecules, present in low concentrations and with low diffusivity, and the capture agents bound to the beads can be increased. For this reason, a coil inspired geometry with a T-inlet has been selected, as this proposal merges two passive mixing strategies: a 3D spiral and a T-junction [35–37]. The T-inlet includes a constriction to increase the turbulence in the meeting point of both streams. The performance of this case is simulated under scenario (ii).

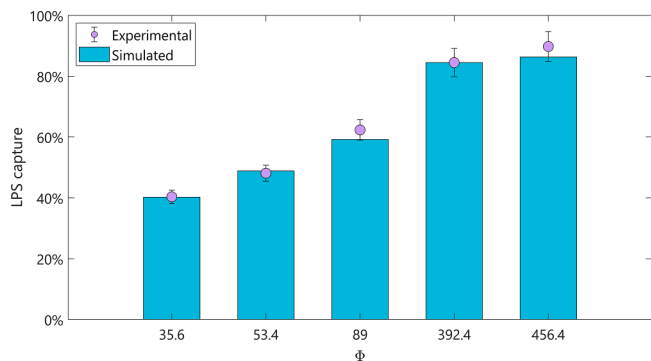


Fig. 4. LPS experimental and simulated capture at different protein:LPS ratios.

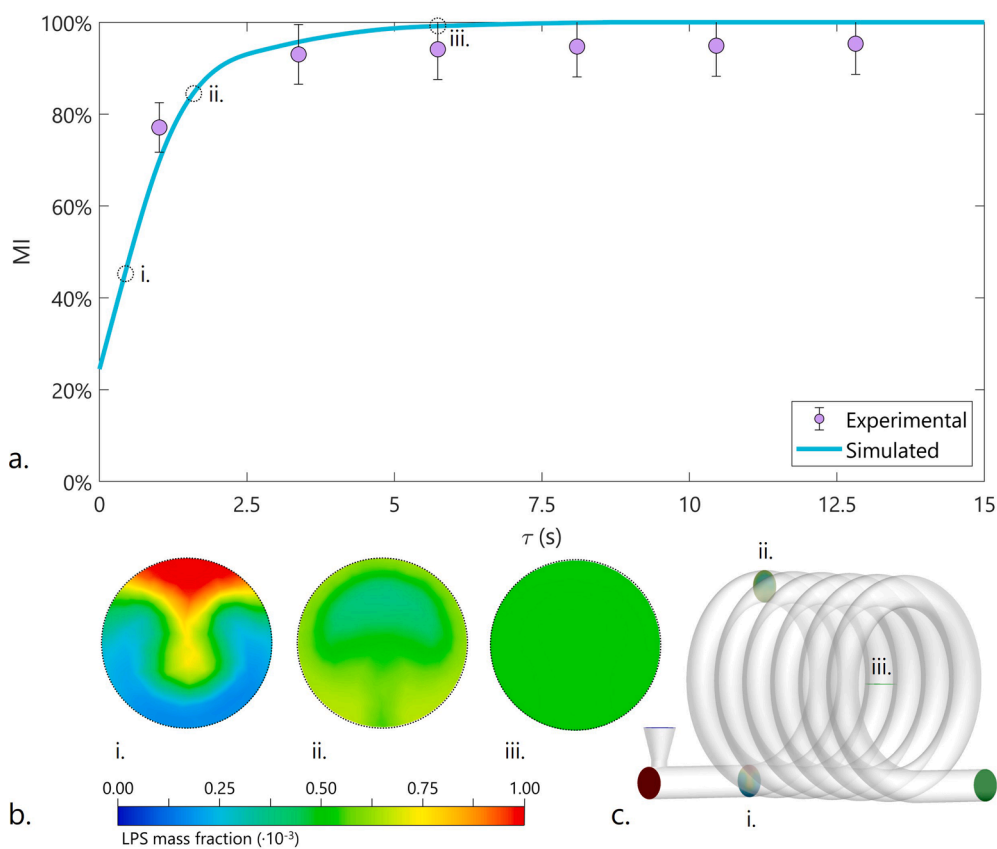


Fig. 5. a. Experimental and simulated progress of the MI along the device, b. LPS concentration contours at a residence time of i. 0.43 s, ii. 1.61 s and iii. 5.74 s and c. Position of the contours in the microdevice.

The mixing efficiency in the proposed device is assessed by selecting 26 cross-sections of the device, including the outlet. In each section, at least 500 sampling points are taken to gather information on the LPS concentration at that position. This data is then used to apply Eq. (26) and calculate the mixing index MI [38]. The experimental and simulated mixing extent through the device is presented in Fig. 5a. The experimental procedure followed to determine the mixing efficiency inside the device can be found in the Supplementary Material. The results point out that the model is able to predict the passive mixing capacity of the device with a deviation (in terms of the RRMSE) inferior to 5 %.

$$MI = 1 - \frac{\left[\sum_{i=1}^N \frac{(c_i - c)^2}{N} \right]^{\frac{1}{2}}}{c} \quad (26)$$

Where N is the number of sampling points in the region of interest, c_i is the concentration in a certain sampling point and c is the complete mixing concentration. The mixing index given as percentage varies from 0 to 100; representing 0 null mixing, while a value of 100 denotes complete mixing.

The suggested configuration guarantees that, when reaching a capacity of 1.4 L per hour, the complete mixing is attained after only 5 s of residence time, proving that the proposed geometry is highly efficient when it comes to blending the liquid phases of two incoming streams and contacting their components. Fig. 5b. shows the LPS concentration contours at different positions. In Fig. 5b.i. the mixing intensity can be appreciated; the inlet structure promotes the mixing by letting one stream envelop the other. This behavior can still be appreciated in Fig. 5b.ii., where both streams have been mixed up to 80 % after less than 2 s. Fig. 5b.iii. displays that after 3 turns in the coil, the fluids are completely mixed.

Another decisive parameter consists of the particle trajectories; the more spread they are through the channel section, the easier the contact with LPS molecules will be. Their positions along the device are depicted in Fig. 6 at different degrees of magnification.

The coil-like main body and the T-inlet constitute a geometry that assures the distribution of the particles through the whole channel (Fig. 6a.). By studying a cross-section of the microreactor (Fig. 6b.) it can be verified that the particles cover the whole diameter of the device and that they tend to move swirling, flowing from the outer part of the channel to the inner part, creating a symmetrical circling scheme. This behavior can be better observed in the magnification provided in Fig. 6c., where the trajectories of the beads lean to create two symmetrical counter-rotating circling structures, whose reason can be found in Fig. 6d. This last image displays the velocity vectors for the fluid in the very same cross-section, which also tend to form two counterrotating circling schemes, well-known as Dean vortices.

The exceptional performance of the designed microdevice in the mixing of the fluids and the wide spreading of the beads sets the best basis for an outstanding LPS capture. Fig. 7 portrays the capture performance of the coiled reactor when it is numerically tested for the S/L reactive contact between LPS and the capturing agents.

Under the selected conditions, the system provides a capture superior to 85 % after a residence time of 15 s. In this case, the removal extent is limited by the capture equilibrium dependant on the selected operational conditions. Moreover, it can be observed, by comparing Figs. 5a. and 7a., that the LPS removal does not take place at a pace as fast as the mixing between both phases. Although the capture kinetics are fast enough to consider the reaction instantaneous, the capture is limited by the mass transfer of the LPS molecules to the proteins bonded to the beads. In any case, the difference between the contours presented in Figs. 5b. and 7b. is notable; the flux scheme is maintained, while the contours are showing colder colours, pointing out to an inferior LPS presence.



Fig. 6. Trajectories of the particles in the microdevice.

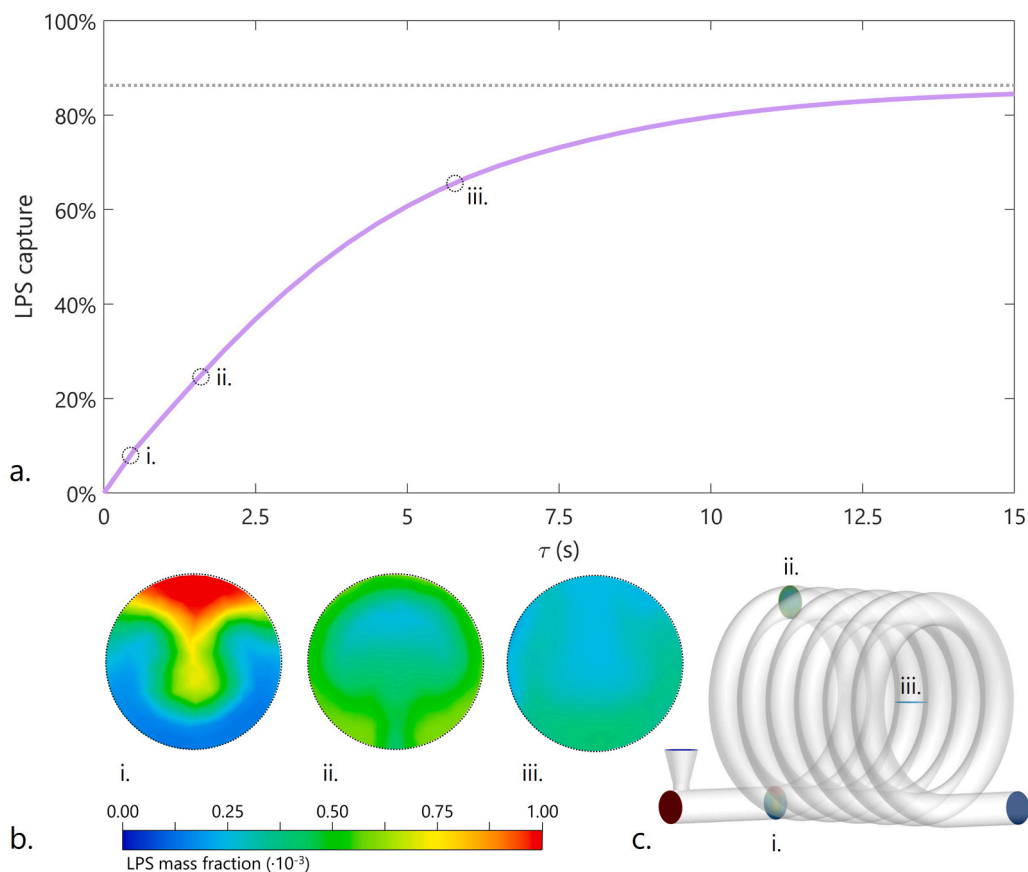


Fig. 7. a. Progress of LPS capture along the device, b. LPS concentration contours at a residence time of i. 0.43 s, ii. 1.61 s and iii. 5.74 s and c. Position of the contours in the microdevice.

5. Conclusions

This work advances the design of high performance microdevices for the selective capture of biomolecules from liquid fluids by creating and developing, to the best knowledge of the authors, the first Eulerian/Eulerian/Lagrangian model devoted to predicting the microfluidic capture of target species onto solid agents. For this purpose, the capture of LPS endotoxin by binding engineered proteins anchored to solid particles is taken as motivating case study. The model herein presented allows to track the solid particles through different fluid phases and accounts for the multiphase mass transfer when the capturing agents and the target species are contacted. The mathematical tool has been successfully validated by replicating batch experiments, with active stirring, containing three phases (air, an LPS aqueous solution and a suspension of beads decorated with engineered binding proteins). Then, the tool has been proved to highly contribute to the design of high performance microdevices for the continuous selective removal of biomolecules from liquid solutions onto engineered particles. For that purpose, a coil-inspired microdevice with a T-inlet has been designed and tested in a biphasic scenario, showing that intensive fluid mixing and uniform distribution of particles are crucial in a scenario in which the target compound is found at very low concentrations and presents reduced mobility. With the proposed geometry and device configuration the LPS capture equilibrium is reached after only 15 s of operation, which can be of great utility in biosensing and bioanalysis applications. Therefore, the mathematical tool herein reported constitutes a new and invaluable assistance in the design of microdevices and microprocesses focused on biosensing molecules whose detection and fast analysis is hindered by their concentration or mobility and for testing S/L removal systems; being easily adaptable and extensible to a vast array of fields of current utmost importance, such as the detection of contaminants of

environmental concern or the impurities in chemical processing.

CRediT authorship contribution statement

Gloria González-Lavín: Writing – original draft, Visualization, Software, Methodology, Investigation, Formal analysis, Data curation, Conceptualization. **Christian Fernández-Maza:** Software, Methodology, Conceptualization. **Lucía Gómez-Coma:** Writing – review & editing, Methodology, Formal analysis, Conceptualization. **Marcos Fallanza:** Writing – review & editing, Supervision, Software, Methodology, Formal analysis, Conceptualization. **Inmaculada Ortiz:** Writing – review & editing, Supervision, Resources, Methodology, Funding acquisition, Formal analysis, Conceptualization.

Declaration of competing interest

The authors declare that they have no known competing financial interests or personal relationships that could have appeared to influence the work reported in this paper.

Acknowledgements

This work received financial assistance from project PID2021-123120OB-I00 funded by MICIU/AEI/ 10.13039/501100011033 and ERDF/EU, and project PDC2022-133122-I00 funded by MICIU/AEI/ 10.13039/501100011033 and the European Union NextGenerationEU/PRTR. Gloria González-Lavín gratefully acknowledges grant FPU21/03297 funded by MICIU/AEI/10.13039/501100011033 and ESF+. The authors also thank the Santander Supercomputacion support group at the University of Cantabria who provided access to the supercomputer Altamira Supercomputer at the Institute of Physics of Cantabria (IFCA-

CSIC), member of the Spanish Supercomputing Network, for performing simulations.

Supplementary materials

Supplementary material associated with this article can be found, in the online version, at [doi:10.1016/j.cej.2025.100747](https://doi.org/10.1016/j.cej.2025.100747).

Data availability

Data will be made available on request.

References

- N. Ma, W. Qiu, G. Wei, J. Zhang, H. Yu, J. Kong, X. Zhang, GOX mediated oxygen tolerance ATRP for detection of esophageal cancer biomarker miRNA-144, *Chem. Eng. J.* 495 (2024), <https://doi.org/10.1016/j.cej.2024.153543>.
- A.C. Fernandes, D. Semenova, P. Panjan, A.M. Sesay, K.V. Germaey, U. Krühne, Multi-function microfluidic platform for sensor integration, *N. Biotechnol.* 47 (2018) 8–17, <https://doi.org/10.1016/j.nbt.2018.03.001>.
- P.S. Chary, S. Shaikh, N. Rajana, V. Bhavana, N.K. Mehra, Unlocking nature's arsenal: nanotechnology for targeted delivery of venom toxins in cancer therapy, *Biomater. Adv.* 162 (2024), <https://doi.org/10.1016/j.bioadv.2024.213903>.
- G. Wang, Y. Ma, X. Zhao, L. Luo, W. Xiu, Z. Jiang, B. Shi, C. Wang, Lignin-assisted local release of triiodothyronine in adipose tissue protects mice against obesity and related metabolic disorders, *Chem. Eng. J.* 496 (2024), <https://doi.org/10.1016/j.cej.2024.153810>.
- G. Ramírez-Guerrero, M. de Cal, A. Lorenzin, D. Vigolo, A.I. Toscano, M. Araya-Rojas, M. Zanella, C. Ronco, Sorbent functionalization with vancomycin enhances bacteria killing in extracorporeal hemoadsorption, *Artif. Organs* 48 (2024) 543–549, <https://doi.org/10.1111/aor.14704>.
- M. Sun, P. Gao, B. Wang, X. Li, D. Shao, Y. Xu, L. Li, Y. Li, J. Zhu, W. Li, Y. Xue, Polydopamine-functionalized selenium nanoparticles as an efficient photoresponsive antibacterial platform, *RSC Adv.* 13 (2023) 9998–10004, <https://doi.org/10.1039/d2ra07737j>.
- J. Gómez-Pastora, I.H. Karampelas, E. Bringas, E.P. Furlani, I. Ortiz, Numerical analysis of bead magnetophoresis from flowing blood in a continuous-flow microchannel: implications to the bead-fluid interactions, *Sci. Rep.* 9 (2019) 7265, <https://doi.org/10.1038/s41598-019-43827-x>.
- A. Basauri, J. Gomez-Pastora, M. Fallanza, E. Bringas, I. Ortiz, Predictive model for the design of reactive micro-separations, *Sep. Purif. Technol.* 209 (2019) 900–907, <https://doi.org/10.1016/j.seppur.2018.09.028>.
- M.B. Plutschack, B. Pieber, K. Gilmore, P.H. Seeburger, The Hitchhiker's Guide to flow chemistry, *Chem. Rev.* 117 (2017) 11796–11893, <https://doi.org/10.1021/acs.chemrev.7b00183>.
- C. Fernández-Maza, G. González-Lavín, L. Gómez-Coma, M. Fallanza, I. Ortiz, High performance flow-focusing droplet microreactor. Extractive separation of rare earths as case of study, *Chem. Eng. J.* 486 (2024) 150136, <https://doi.org/10.1016/j.cej.2024.150136>.
- M. Madadelahi, L.F. Acosta-Soto, S. Hosseini, S.O. Martinez-Chapa, M.J. Madou, Mathematical modeling and computational analysis of centrifugal microfluidic platforms: a review, *Lab. Chip.* 20 (2020) 1318–1357, <https://doi.org/10.1039/C9LC00075J>.
- O. Mahian, L. Kolsi, M. Amani, P. Estellé, G. Ahmadi, C. Kleinstreuer, J.S. Marshall, M. Siavashi, R.A. Taylor, H. Niazmand, S. Wongwises, T. Hayat, A. Kolanjiyil, A. Kasaeian, I. Pop, Recent advances in modeling and simulation of nanofluid flows-part I: fundamentals and theory, *Phys. Rep.* 790 (2019) 1–48, <https://doi.org/10.1016/j.physrep.2018.11.004>.
- G. González-Lavín, B. García-Merino, C. Fernández-Maza, E. Bringas, L. Gómez-Coma, M. Fallanza, I. Ortiz, Tailored Euler-Lagrange modelling of microfluidic solid/liquid reactive separations, *Chem. Eng. J.* 495 (2024) 153393, <https://doi.org/10.1016/j.cej.2024.153393>.
- B.G.M. van Wachem, A.E. Almdstedt, Methods for multiphase computational fluid dynamics, *Chem. Eng. J.* 96 (2003) 81–98, <https://doi.org/10.1016/j.cej.2003.08.025>.
- R.S.S. Raja Ehsan Shah, B. Sajjadi, A.A. Abdul Raman, S. Ibrahim, Solid-liquid mixing analysis in stirred vessels, *Rev. Chem. Eng.* 31 (2015) 119–147, <https://doi.org/10.1515/revce-2014-0028>.
- P. Roy, L.-W.A. Chen, Y.-T. Chen, S. Ahmad, E. Khan, M. Buttner, Pollen dispersion and deposition in real-world urban settings: a computational fluid dynamic study, *Aerosol Sci. Eng.* 7 (2023) 543–555, <https://doi.org/10.1007/s41810-023-00198-1>.
- F. Huang, Y. Zhang, Z.B. Tong, X.L. Chen, R.Y. Yang, A.B. Yu, Numerical investigation of deposition mechanism in three mouth-throat models, *Powder. Technol.* 378 (2021) 724–735, <https://doi.org/10.1016/j.powtec.2018.11.095>.
- L. Xu, Q. Zhang, J. Zheng, Y. Zhao, Numerical prediction of erosion in elbow based on CFD-DEM simulation, *Powder. Technol.* 302 (2016) 236–246, <https://doi.org/10.1016/j.powtec.2016.08.050>.
- P. Bhardwaj, P. Bagdi, A.K. Sen, Microfluidic device based on a micro-hydrocyclone for particle-liquid separation, *Lab. Chip.* 11 (2011) 4012, <https://doi.org/10.1039/c1lc20606k>.
- C. Suvanjumrat, P. Phrommark, J. Chaiyanupong, J. Priyadumkol, T. Phengpom, W. Chookaew, P. Tekasakul, K. Inthavong, M. Promtong, CFD analysis of microscopic particle separation in low-volumetric classifiers: DPM tracking and experimental validation for enhanced efficiency using geometric modification strategy, *Chem. Eng. J.* 502 (2024) 157997, <https://doi.org/10.1016/j.cej.2024.157997>.
- M. Massoudi Farid, H.J. Jeong, K.H. Kim, J. Lee, D. Kim, J. Hwang, Numerical investigation of particle transport hydrodynamics and coal combustion in an industrial-scale circulating fluidized bed combustor: effects of coal feeder positions and coal feeding rates, *Fuel* 192 (2017) 187–200, <https://doi.org/10.1016/j.fuel.2016.12.025>.
- Y. Xu, B. Jin, Y. Zhao, E.J. Hu, X. Chen, X. Li, Numerical simulation of aqueous ammonia-based CO₂ absorption in a sprayer tower: an integrated model combining gas-liquid hydrodynamics and chemistry, *Appl. Energy* 211 (2018) 318–333, <https://doi.org/10.1016/j.apenergy.2017.11.054>.
- Y. Yang, H. Zhang, A.C. Lai, Lagrangian modeling of inactivation of airborne microorganisms by in-duct ultraviolet lamps, *Build. Environ.* 188 (2021), <https://doi.org/10.1016/j.buildenv.2020.107465>.
- F. Barbosa, J. Dueñas-Pamplona, C.S. Abreu, M.S.N. Oliveira, R.A. Lima, Numerical model validation of the blood flow through a microchannel hyperbolic contraction, *Micromachines*. (Basel) 14 (2023) 1886, <https://doi.org/10.3390/mi14101886>.
- A. Shiriny, M. Bayareh, Inertial focusing of CTCs in a novel spiral microchannel, *Chem. Eng. Sci.* 229 (2021) 116102, <https://doi.org/10.1016/j.ces.2020.116102>.
- Q. Yang, D. Ju, Y. Liu, X. Lv, Z. Xiao, B. Gao, F. Song, F. Xu, Design of organ-on-a-chip to improve cell capture efficiency, *Int. J. Mech. Sci.* 209 (2021) 106705, <https://doi.org/10.1016/j.ijmecsci.2021.106705>.
- A. Basauri, M. Fallanza, L. Giner-Robles, R. Fernandez-Lopez, G. Moncalián, F. de la Cruz, I. Ortiz, Integrated strategy for the separation of endotoxins from biofluids. LPS capture on newly synthesized protein, *Sep. Purif. Technol.* 255 (2021) 117689, <https://doi.org/10.1016/j.seppur.2020.117689>.
- A. Basauri, Advanced methodology for LPS capture from biofluids, PhD. Thesis. University of Cantabria, <http://hdl.handle.net/10902/21926>, 2021.
- Ansys® Fluent, Release 2024R1, Ansys Fluent User's Guide.
- A. Li, G. Ahmadi, Dispersion and deposition of spherical particles from point sources in a turbulent channel flow, *Aerosol Sci. Technol.* 16 (1992) 209–226, <https://doi.org/10.1080/02786829208959550>.
- S.A. Morsi, A.J. Alexander, An investigation of particle trajectories in two-phase flow systems, *J. Fluid Mech.* 55 (1972) 193–208, <https://doi.org/10.1017/S0022112072001806>.
- K.K. Sirkar, Creeping flow mass transfer to a single active sphere in a random spherical inactive particle cloud at high schmidt numbers, *Chem. Eng. Sci.* 29 (1974) 863–869, [https://doi.org/10.1016/0009-2509\(74\)80206-X](https://doi.org/10.1016/0009-2509(74)80206-X).
- C.J. Thomas, B.P. Gangadhar, N. Suroliya, A. Suroliya, Kinetics and mechanism of the recognition of endotoxin by polymyxin B, *J. Am. Chem. Soc.* 120 (1998) 12428–12434, <https://doi.org/10.1021/ja981777j>.
- H.A. Radi, J.O. Rasmussen, Principles of Physics, Springer Berlin Heidelberg, Berlin, Heidelberg, 2013. <https://doi.org/10.1007/978-3-642-23026-4>.
- C.-Y. Lee, W.-T. Wang, C.-C. Liu, L.-M. Fu, Passive mixers in microfluidic systems: a review, *Chem. Eng. J.* 288 (2016) 146–160, <https://doi.org/10.1016/j.cej.2015.10.122>.
- H. Shi, K. Nie, B. Dong, M. Long, H. Xu, Z. Liu, Recent progress of microfluidic reactors for biomedical applications, *Chem. Eng. J.* 361 (2019) 635–650, <https://doi.org/10.1016/j.cej.2018.12.104>.
- C. Fernández-Maza, M. Fallanza, L. Gómez-Coma, I. Ortiz, Performance of continuous-flow micro-reactors with curved geometries. Experimental and numerical analysis, *Chem. Eng. J.* 437 (2022) 135192, <https://doi.org/10.1016/j.cej.2022.135192>.
- R.A. Taheri, V. Goodarzi, A. Allahverdi, Mixing performance of a cost-effective split-and-recombine 3D micromixer fabricated by xurographic method, *Micromachines* (2019) 10, <https://doi.org/10.3390/mi10110786>.